Mineralium Deposita (1998) 34: 4–18

ARTICLE

F. Velasco · J. Sánchez-España · A. J. Boyce
A. E. Fallick · R. Sáez · G. R. Almodóvar

A new sulphur isotopic study of some Iberian Pyrite Belt deposits: evidence of a textural control on sulphur isotope composition

Received: 8 October 1997 / Accepted: 14 May 1998

Abstract The sulphide deposits of the Iberian Pyrite Belt (IPB) represent an ore province of global importance. Our study presents 113 new sulphur isotope analyses from deposits selected to represent the textural spectrum of ores. Measured $\delta^{34}S$ values range from -26 to $+10‰$ mostly for massive and stockwork ores, in agreement with data previously published. In situ laser $\delta^{34}S$ analyses reveals a close correlation of $\delta^{34}S$ with texture. Primary diagenetic textures are dominated by relatively low $\delta^{34}S$ ($-8‰$ to $-2‰$), whereas stockwork feeder textures are dominated by higher $\delta^{34}S$ ($\sim +3‰$ to $+5‰$). Intermediate textures (mainly coarse textures in stratiform zones) have intermediate $\delta^{34}S$, although they are mostly dominated by the high $\delta^{34}S$ component. Rare barite has a homogeneous $\delta^{34}S$ around $+18‰$, which is consistent with direct derivation from Lower Carboniferous seawater sulphate. A dual source of sulphide sulphur in the IPB deposits has been considered. A hydrothermal source, derived from reduction of coeval seawater sulphate in the convective systems, is represented by sulphide in the feeder zones. Here variations in $\delta^{34}S$ are caused by variations in the extent of the sulphate reduction, which governs the SO_4:H_2S ratio. The second end-member was derived from the bacterial reduction of coeval seawater sulphate at or near the surface, as reflected in the primary textures. A distinct geographical variation in $\delta^{34}S$ and texture from SW (more bacteriogenic and primary textures) to NE (more hydrothermal textures and $\delta^{34}S$) which reflects a variation in the relative input of each source was likely controlled by local geological environments. Given that the sulphur isotope characteristics of the IPB deposits are unlike most VMS and Kuroko deposits, and noting the dominance of a mixed reduced sedimentary and volcanic environment, we suggest that the IPB could represent an ore style which is intermediate between volcanic and sedimentary hosted massive sulphide types.

Editorial handling: T. Grenne · T. Bjerkgård

F. Velasco (✉) · J. Sánchez-España
Departamento de Mineralogía y Petrología,
Universidad del País Vasco, Apdo. 644.
E-48080 Bilbao, Spain

A.J. Boyce · A.E. Fallick
Isotope Geosciences Unit, SURRC,
East Kilbride, Glasgow, G75 0QF,
Scotland, UK

R. Sáez · G.R. Almodóvar
Departamento de Geología, Universidad de Huelva,
E-21819 La Rábida (Huelva), Spain

Introduction

The Iberian Pyrite Belt (IPB) volcanic- and sediment-hosted deposits are regarded as one of the world's major massive sulphide provinces, and include several noted giant orebodies with reserves of some hundreds of million tons (e.g. Rio Tinto, Neves Corvo, Aljustrel, Tharsis, Sotiel, Aznalcollar; Fig. 1). These deposits were formed as consequence of intense hydrothermal activity during Upper Devonian to Lower Carboniferous times, when felsic and mafic lavas and tuffs, volcanic breccias, and sediments, such as shales, quartzites, greywackes, limestones and cherts, were deposited (Sáez et al. 1996). The massive sulphides and the host rocks were later variably metamorphosed and deformed during the Hercynian orogeny. Considering the close relationship to felsic volcanism and some other geological features, several authors have classified the IPB massive sulphide deposits as Kuroko type (Hutchinson 1983; Sawkins 1990). However, it seems that an Iberian type (Sáez et al. in press) of massive sulphide deposits is more appropriate, because the importance and general features of the province (e.g. the peculiarities about the sulphur isotope composition). Whatever their classification, there is little doubt that most of these sulphides were precipitated on or near the coeval sea floor, during the waning stages of volcanic activity (Barriga 1990; Sáez et al. 1996).

In the last three decades, approaching 500 sulphur isotopic analyses have been carried out mainly on the

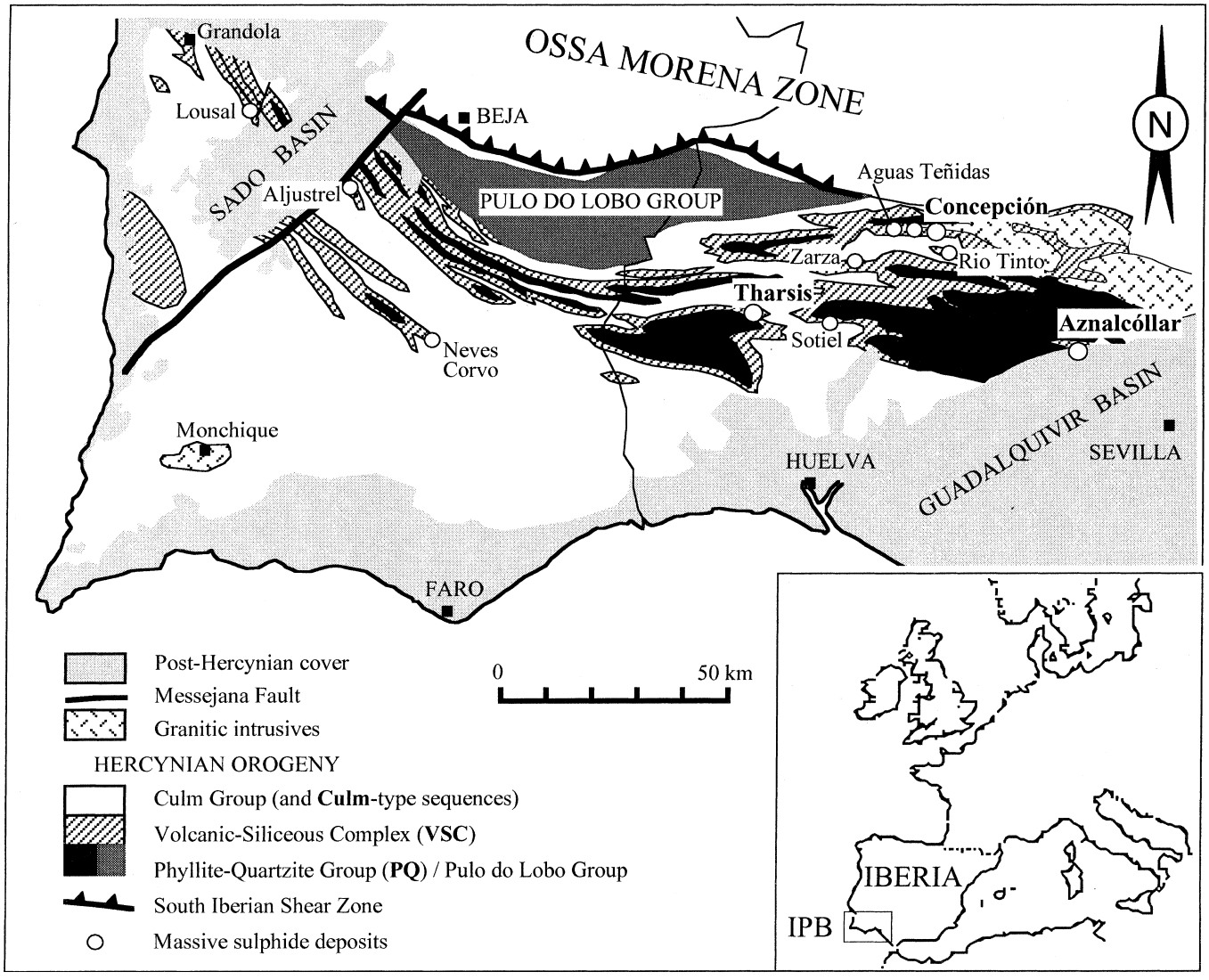

Fig. 1 Simplified geological map of the Iberian Pyrite Belt showing the location of the deposits studied (adapted from Carvalho et al. 1976)

massive and stockwork ores of IPB deposits (Rambaud 1969; Williams et al. 1975; Arnold et al. 1977; Lécolle 1977; Routhier et al. 1978; Eastoe et al. 1986; Mitsuno et al. 1988; Kase et al. 1990; Yamamoto et al. 1993; Almodóvar et al. 1998; Tornos et al. 1998). Whilst sulphides in many volcanogenic massive sulphide (VMS) deposits show generally positive $\delta^{34}S$ values, with a close relationship to $\delta^{34}S$ of coeval seawater sulphate, IPB sulphides exhibit a wide variation of $\delta^{34}S$ values, both positive and negative among different deposits, and even within the same deposit (Table 1; Fig. 2). The majority of the massive ores, mostly composed of pyrite, yield a widely scattered distribution, ranging from $-34‰$ to $+15‰$ with an average close to $0‰$ (e.g. Aljustrel, Aznalcollar, Sotiel, Neves-Corvo). Only San Telmo displays a narrow range of positive values ($+0.5$ to $+4.9‰$, according to Mitsuno et al. 1988). Vein-stockwork ores clearly exhibit mostly positive isotopic values (average of $+4.7‰$). Barite is rare in the IPB deposits (found to date only in San Telmo, San Dionisio, Sierrecilla, San Platón and Planes: Routhier et al. 1978; García de Miguel 1990) with average $\delta^{34}S$ around $+18‰$ (Eastoe et al. 1986; Mitsuno et al. 1988; this study). The scarcity of barite is a feature which marks a distinction with Kuroko deposits, and indicates a relatively reduced environment of deposition, with only minor changes in the oxidation state of the fluids during massive sulphide deposition (Rye and Ohmoto 1974). Tables 1 and 2 summarize the available data.

Controversy exists about whether VMS deposits were formed by magmatic, connate or convective seawater hydrothermal systems or some mixture thereof. Sulphur isotope studies have proposed two potential sources for the deposits: either magmatic sulphur derived from sulphides within associated igneous rocks (Rambaud 1969; Williams et al. 1975), or a reduced seawater source (Lécolle 1977; Routhier et al. 1978; Mitsuno et al. 1988; Kase et al. 1990; Yamamoto et al. 1993). The latter

Table 1 Selected sulphur isotope data in ‰ $\delta^{34}S$ from literature on principal massive sulphide deposits and main host rocks from IPB

Group	Number	Mean	Median	SD	Minimum	Maximum
1 Tharsis	73	−4.3	−4.5	3.6	−26.8	3.5
2 Loussal	15	−2.0	−3.0	4.2	−8.3	5.5
3 Aljustrel	41	−1.7	−1.3	4.4	−20.4	4.0
4 Sotiel	35	−4.7	−0.7	12.6	−34.2	6.7
5 Aznalcóllar	16	−0.1	0.3	2.9	−6.0	4.4
6 Neves Corvo	51	1.1	1.6	3.6	−11.1	6.0
7 La Zarza	32	0.8	0.4	2.9	−7.3	7.8
8 Lomero Poyatos	8	2.7	3.4	1.5	−0.1	3.9
9 San Miguel	13	2.1	2.8	4.3	−3.9	9.2
10 San Telmo	14	3.0	3.2	1.3	0.5	4.9
11Rio Tinto	121	4.3	5.0	4.7	−14.1	12.4
12 Concepción	10	5.4	6.0	3.4	−1.4	9.2
Stockwork	51	4.7	4.6	4.3	−4.5	11.7
Jaspers	4	−23.7	−27.8	11.4	−32.1	−7.0
Slates	13	−2.1	−3.1	6.8	−16.6	6.7
Volcanic rocks	8	−2.5	−2.1	5.0	−10.0	6.5
Total IPB data						
Sulphides[a]	468	−0.2	0.8	7.1	−34.2	12.4
Barite	9	17.8	16.0	3.3	14.9	24.0

Source of data analysis: Rambaud (1969), Arnold et al. (1977), Lécolle (1977), Eastoe et al. (1986), Mitsuno et al. (1988), Kase et al. (1990), Yamamoto et al., 1993, and Tornos et al., (1998)

[a] Data analysis belonging to sulphides from some minor deposits have not been included

hypothesis allows a variable contribution from both reduction of seawater in the hydrothermal system, and also from bacterial reduction near the site of deposition.

All of these cited sulphur isotopic studies were performed using conventional techniques. Most of the studies acknowledge that, because of the fine-grained and complex nature of the ores, mixed sulphides were analyzed. Thus, these studies give us the average $\delta^{34}S$ of the main co-existing sulphide minerals. However, recent studies (Eldridge et al. 1988, 1993; Kelley and Fallick

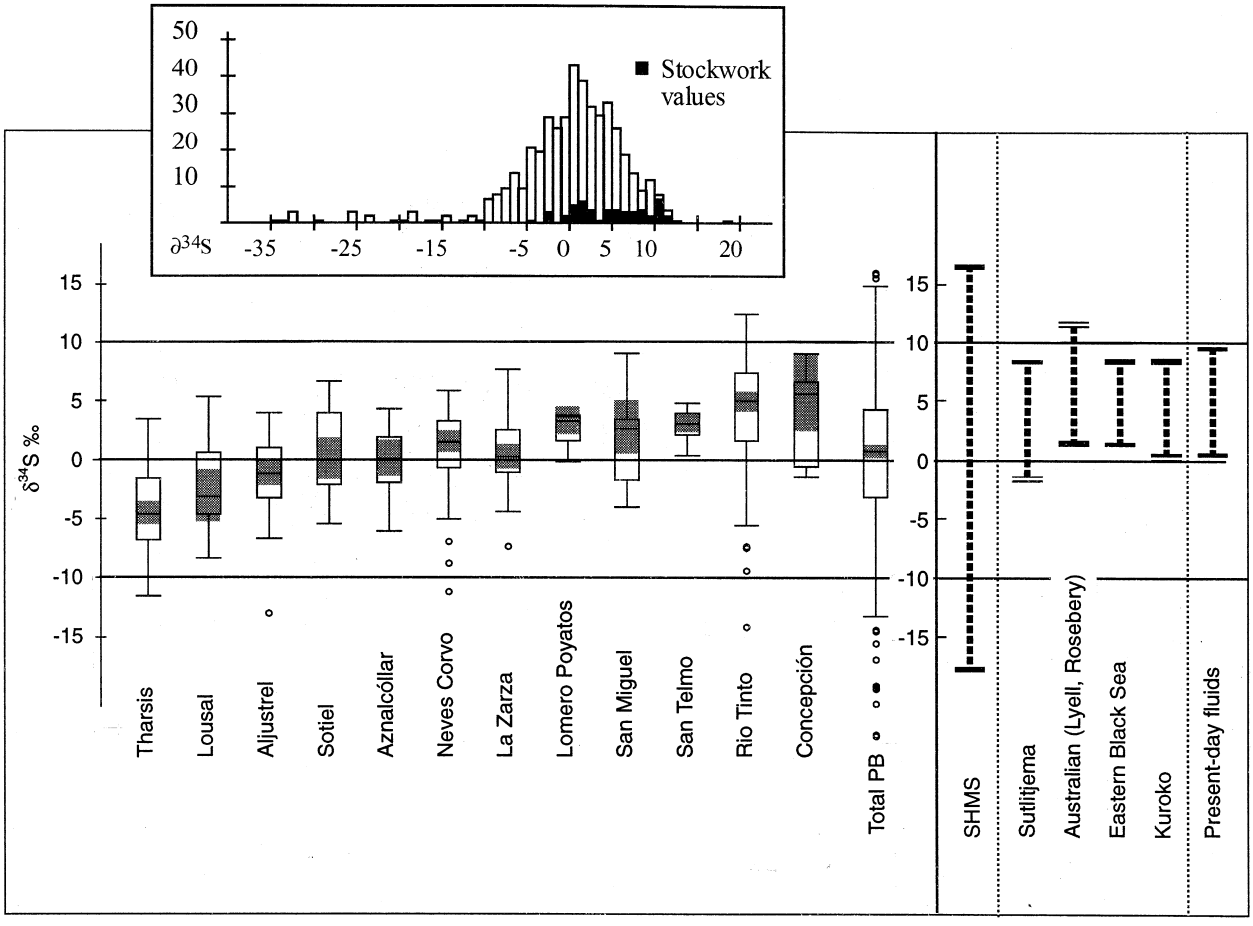

Table 2 Reported sulphur isotope studies on ores from the IPB deposits

Reference	*n*	Main suggested source of sulphur	Remarks
Rambaud (1969)	27	Magmatic (juvenile)	Sulphur signature modified by isotopic exchange with sulphur of seawater derivation
Williams et al. (1975)	(27)	Juvenile fluids modified by mixing with hot sulphate-bearing seawater	These authors use the same isotope data presented by Rambaud (1969)
Arnold et al. (1977)	47	Hydrothermal exhalative	Inorganic reduction of coeval seawater sulfates and leaching of the sulphides disseminated in the host volcanic rocks
Routhier et al. (1978)	32	Bacteriogenic fractionation from a deep sulphur source	Progressive influence of marine environment. Data come mainly from the PhD Thesis by Lécolle (1977)
Eastoe et al. (1986)	32	Hydrothermal fluids	Derived from contemporaneous seawater sulphate ± inputs of biogenic sulphur in the margins of stratiform bodies and in stockwork
Mitsuno et al. (1988)	300	Bacteriogenic	High variability of sulphur isotopes: stockwork ores largely derived from volcanogenic sulphur while layered ores derived from mixture of volcanogenic and bacteriogenic sulphur
Kase et al. (1990)	30	Bacteriogenic and connate	Applied to the Tharsis deposit. Stockwork sulphur is largely volcanogenic and cognate with the original sulphur in the felsic rocks
Yamamoto et al. (1993)	14	Bacteriogenic and volcanogenic	Influence of sulphate/sulphide ratio in the fluids due to changes in *f*O2 and pH condition during ore deposition. Stockwork largely volcanogenic; massive ores from mixture of volcanogenic and bacteriogenic sulphur
Tornos et al. (1998)	14	Bacteriogenic	Most of the sulphur was bacteriogenically reduced before reacting with hydrothermal brines

n, number of samples analyzed using conventional mass spectrometric methods

1990) indicate that in situ sulphur isotopic analyses at moderate to high resolution can reveal genetically significant information which can not be caption Fig. 2 discerned using the bulk conventional techniques. Accordingly, our study aims to describe the common textural features of sulphide ores from the IPB deposits, and to use conventional and laser-based isotope analyses to distinguish the isotopic compositions of sulphides from the various stages of deposition, hydrothermal replacement and metamorphism. This is the first in situ laser sulphur isotope study of Iberian sulphides. Using existing isotopic data and our new petrographic studies, we have selected several deposits which cover the isotopic and textural spectrum of the IPB. These include the giant Tharsis deposit (Fig. 1: the lowest $\delta^{34}S$ end-member, and the least metamorphosed of our selected group) and Concepción (the highest $\delta^{34}S$ end-member, with the most abundant secondary textures). What emerges from our study is a close correlation of $\delta^{34}S$ with texture, which allows elucidation of genetic models for these deposits.

Fig. 2 Plot of the available conventional $\delta^{34}S$ data for the main ore deposits from the Iberian Pyrite Belt (Rambaud 1969; Williams et al. 1975; Arnold et al. 1977; Lécolle. 1977; Routhier et al. 1978; Eastoe et al. 1986; Mitsuno et al. 1988; Kase et al. 1990; Yamamoto et al. 1993; Tornos et al. in press) shown with increasing mean $\delta^{34}S$ to the *right* of the diagram. Deposits have been organized considering their geographic location (approximately from SW to NE) and their respective $\delta^{34}S$ averages (from lower to higher $\delta^{34}S$ values). IPB *boxplot* represents all the published sulphur isotope data, including sulphides from ores and host rocks. Boxplots define the median (*horizontal line across the box*), percentiles, whiskers, and outliers; *shaded area* on each box indicates 95% confidence interval bounds around its median. For comparison purposes common ranges of $\delta^{34}S$ values for the sediment-hosted massive sulphide deposits (SHMS), some selected volcanic hosted sulphide massive deposits, and the present-day mid-ocean hydrothermal fluids have been plotted (data from Ohmoto and Rye 1979; Eldridge et al. 1988; Bluth and Ohmoto 1988; Cagatay and Eastoe 1995; Ohmoto 1996; Cook and Hoefs 1997; Herzig 1997)

Geological setting

The sampled deposits (Fig. 1) are located in the central and eastern part of the IPB, which is the main region of the South Portuguese Zone of the Iberian Hercynian orogene. This belt extends over a distance of 230 km from Seville (in Spain) to the south of Lisbon (in Portugal), with a width of about 30 km; it delineates an E-W

striking structure in Spain, changing to NW-SE in Portugal. The stratigraphic sequence comprises several conformable sedimentary successions of late Devonian to Carboniferous age (Strauss 1970; Carvalho et al. 1976; Routhier et al. 1978; Barriga 1990; Sáez et al. 1996) including several intercalated acid and basic volcanic units of Dinantian age (Routhier et al. 1978; Munhà 1983; Thiéblemont et al. 1994) and the presence of the huge massive sulphide deposits (Sáez et al. 1996).

Three main lithostratigraphic units have been established in the IPB (Schermerhorn 1971), which from older to younger are:

1. The Phyllite-Quartzite Group (PQ), composed of Upper Devonian slates, quartzites and litharenites;
2. The Volcano-Sedimentary Complex (VSC), Upper Devonian to Middle Visean in age, comprising felsic and mafic volcanic rocks interbedded with detrital sediments, and hosting the massive sulphide deposits;
3. The Culm Group, composed of a flysch-like turbiditic sequence of slates and sandstones of Upper Visean to Lower Westphalian age.

In the VSC, three main felsic volcanic events are usually distinguished alternating with two mafic ones. These volcanic units are generally intercalated in pelitic rocks. As a general rule, the majority of the massive sulphide deposits of the southern zones are associated with the top of the first (V1) felsic volcanic episode, whereas deposits located in the northern zone are mainly associated with the second (V2) felsic volcanic episode (Routhier et al. 1978; Sáez and Almodóvar 1993; Sáez et al. 1996; Sáez et al. in press). The host rocks are mainly tuffs and lava flows of dacitic to rhyolitic composition (Almodóvar and Sáez 1992; Sáez et al. 1996) with terrigenous sediments, including black shales. Volcanic rocks show a monotonous mineralogy, with quartz and albite phenocrysts supported by a quartz-feldspar-sericite groundmass. In most cases, the original volcanic textures are preserved, only being obliterated where deformation or hydrothermal alteration is most intense.

These rocks were folded and metamorphosed during the Hercynian orogeny, under conditions of very low to low-grade metamorphism (Schermerhorn 1971; Munhá 1983, 1990). In addition, and prior to the low-grade metamorphism, VSC rocks underwent a regional hydrothermal alteration (Munhá and Kerrich 1980; Barriga 1990), as well as a more local and intense hydrothermal alteration contemporaneous with the deposition of the massive sulphides, resulting in intense chloritization and sericitization of the wall rocks (Barriga 1990; Toscano et al. 1993; Almodóvar et al. 1995; Sáez et al. 1996; Sánchez-España et al. 1997).

Although some synsedimentary tectonic events have been reported in relation to basin subsidence (Moreno et al. 1996), the main stages of deformation (D1, D2 and D3) recognized in the IPB are clearly associated with the Hercynian orogeny (Ribeiro and Silva 1983; Quesada 1991). The principal compressive deformation (D1), accompanied by regional metamorphism, produced tight folds, thrusts and overthrusts. The regional variability in the intensity of the deformation and metamorphism is related to proximity of shear zones.

Ore petrography

Despite the occurrence of a great number of minor, trace and very rare minerals, the major ore mineralogy of the IPB deposits is relatively simple (Strauss 1970; Routhier et al. 1978; García de Miguel. 1990; Marcoux et al. 1996). The dominant mineral is pyrite, accompanied by subordinate chalcopyrite, sphalerite and galena. Tetrahedrite, arsenopyrite, pyrrhotite and cassiterite often occur in significant, but minor quantities, most commonly in the stringer assemblages. A range of bismuth sulphides, sulphosalts and rare cobalt sulphoarsenides are characteristic indicators of these stringer zones

►

Fig. 3A–F Polarized reflected-light photomicrographs of some ore samples used in this study showing primary and secondary textures with examples of coexisting low and high $\delta^{34}S$ values (*figures* in ‰). The scale bar is 200 μm in all photos. **A** Bedded pyritic ore consisting of fine-grained pyrite laminae, flattened framboids and pyrite spheroids surrounded by a radial fibrous rim, Tharsis deposit. Specimen etched with HNO_3. **B** Pyrite framboids surrounded by recrystallized sphalerite (*sp*) and disseminated euhedral pyrite crystals. Neoblasts of sphalerite displaying abundant annealing and some deformation twins. Concepción mine. Specimen etched with HNO_3. **C** Replacement texture of primary colloform and crustiform pyrite (*white*) with relict radial and concentric growth structures, sieved with sphalerite (*dark grey*) and galena (*light grey*, *gn*), Aznalcóllar mine. **D** Coarse-grained euhedral pyrite crystals containing relict of zoned cores (framboids?) replaced by sphalerite and enveloped in a matrix of sphalerite (*dark grey*) and gangue minerals (*black*), Aznalcóllar mine. **E** Deformed pyrite metablasts separated by gangue (mainly carbonates) showing sutured grain boundaries, brecciation and the effects of pressure solution. Concepción deposit. Specimen etched with HNO_3. **F** Recrystallized massive pyrite showing strongly indented grains enveloping a lens of magnetite (*mt*). Truncated grain boundaries by pressure solution develop a preferred shape orientation, Concepción deposit. Specimen etched with HNO_3

(Marcoux et al. 1996). In some deposits, magnetite or pyrrhotite occur as minor minerals, though the magnetite may locally be very abundant (e.g. Castillo de las Guardas, Concepción). Quartz, carbonate, muscovite and chlorite are the most common gangue minerals.

Four main ore facies have been distinguished (massive, banded, breccia and stringer ores) within each deposit. However, despite these various ore types, a continuous spectrum of sulphide assemblages and textural characteristics can be established.

In order to evaluate the wide textural range displayed by pyrite ores, three different types of deposits have been studied: (1) the first is characterized by the predominance of the original sedimentary-diagenetic features (e.g. Tharsis); (2) the second includes the more overprinted, deformed and metamorphosed orebodies with very rare sedimentary features (e.g. Concepción); and (3) all the intermediate cases (e.g. Aznalcóllar), characterized by massive ores displaying relicts of primary depositional textures together with variable hydrothermal and deformational effects. In all the studied deposits ores show extremely variable textures, with marked textural changes observed over very short distances (sometimes less than 1 mm in the same sample). We have established the following textural groupings:

(1) *Growth textures*: early pyrite exhibits nodular or crustiform microstructures usually as dense and massive subautomorphic growths, or disseminated single grains. These include framboidal, colloform, spheroidal, with shrinkage or syneresis cracks, and microcrystallite textures (Fig. 3A,B). Framboidal and colloform pyrite could have been formed by colloidal precipitation (Papunen 1966; Ramdohr 1980), but may also be due to crystallization from supersaturated solutions (Roedder 1968). Complex growth processes involving magnetic attraction and aggregation of magnesioferrite (Taylor 1982), or several stages of nucleation, aggregation and replacement of greigite by pyrite (Wilkin and Barnes

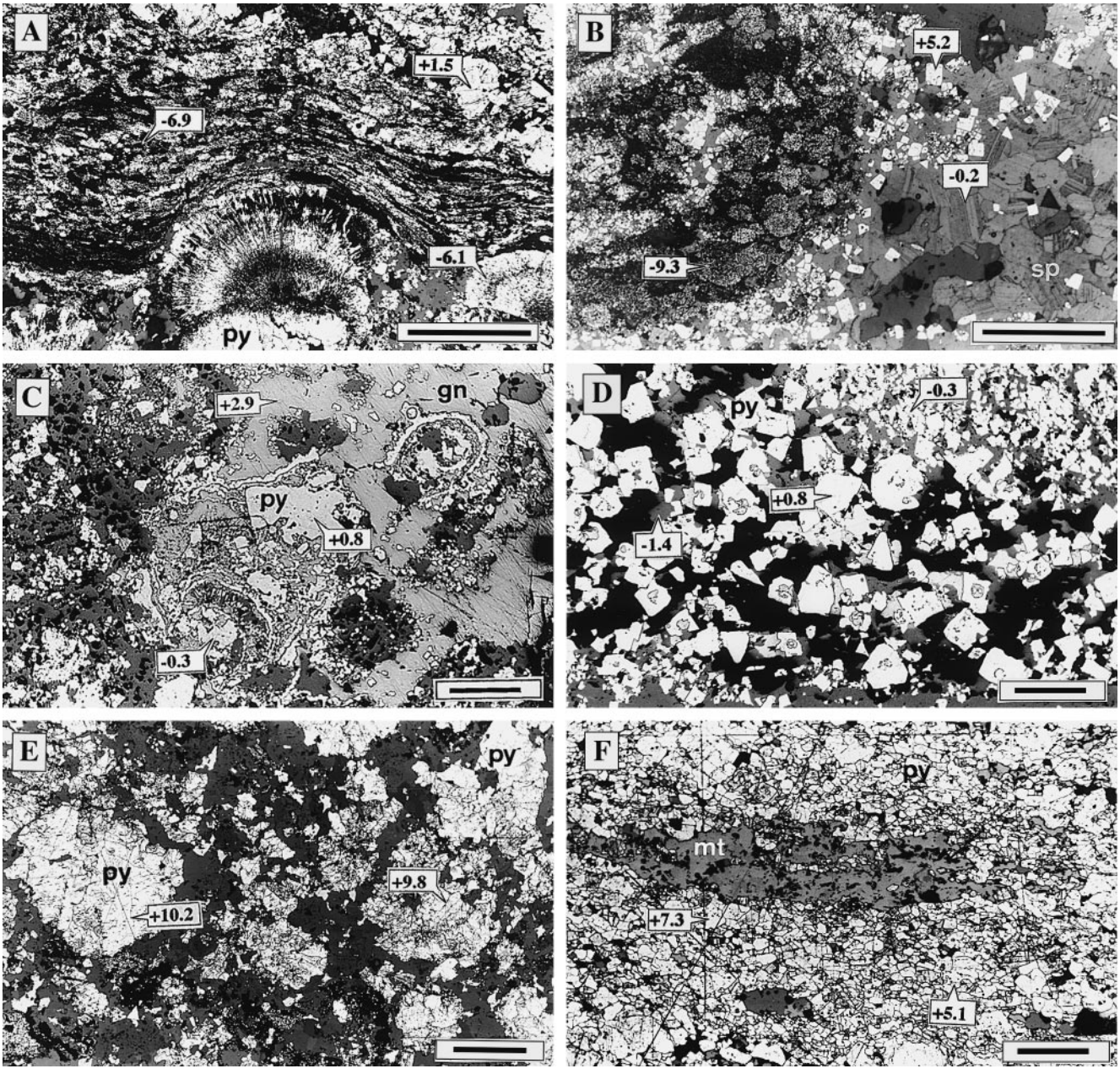

1997), have recently been proposed to explain pyrite framboid formation at low to moderate temperatures.

(2) *Replacement textures*: hydrothermal replacement during deposition and late diagenesis is commonly the principal factor responsible for the obliteration of early textures. Replacement of ''gel-pyrite'' (melnikovite) or other initially ''dusty'' pyrite forms by idiomorphic habits and ''birds-eye'' textures, with matrix of chalcopyrite are very frequent. This secondary pyrite shows zoned overgrowths, subhedral to euhedral crystals, and impingement overgrowths (McClay 1991; Lianxing and McClay 1992). The cores of the crystals frequently exhibit spongy pyrite perhaps as a result of recrystallization of polyframboid pyrite aggregates, whereas the inclusion free euhedral pyrite crystals appear as a concentric rim on the automorphic crystals (Fig. 3C,D). Pyrite from the stockwork zones also display euhedral morphologies and coarse-grained textures.

(3) *Deformation and metamorphic textures*: the effects of deformation and metamorphism on sulphide are variable, even within a single deposit. Pyrite shows a general tendency towards cataclasis, whereas sphalerite and chalcopyrite and galena show a variety of texture indicative of ductile deformation (Cox 1987; McClay 1991; Lianxing and McClay 1992; Pesquera and Velasco 1993). In general, in pyrite ores the following features can be observed: (1) microfracturing and blow-apart effects, (2) porphyroclastic textures, (3) non-equilibrium impingement microstructures with a variable grain size, irregular boundaries and multiple junctions, and (4)

granoblastic textures and elongated pyrite grains whose origin is debatable (Fig. 3E,F). Granular metablastic pyrite, composed of fine to very fine-grained metacrystals developed during metamorphic recrystallization, are also free of inclusions, being surrounded by a coarse-grained matrix comprising recrystallized sphalerite crystals, and other gangue minerals. Additionally, accompanying ductile sulphides, such as sphalerite, chalcopyrite and galena, have often been dynamically recrystallized.

Massive ores representative of the first type of deposits (Tharsis deposit, Filón Norte) display numerous free-growth habits, being dominantly framboidal, colloform and spherulitic textures. These morphologies are typical of the sedimentary or early diagenetic environments mainly formed at relatively low temperatures (stage I, Fig. 4). The intermediate or transitional type of deposits (e.g. Aznalcóllar) are recognized by the presence of replacement, "atoll" and "birds-eye" textures, equi-dimensional habits and by the presence of finely disseminated automorphic pyrite microcrystallites. Impingements (formed by interaction of competing pyrite overgrowths, to form monomineralic massive aggregates), zoning and diagenetic overgrowths (normally involving a central pyrite micrograin with secondary pyrite overgrowths) are common. These features represent a continuum from early primary textures (stage I) to the late hydrothermal replacements (stage II, Fig. 4), indicating that the primary minerals and textures have been replaced and refined by later fluids, presumably at higher temperature. The most deformed deposits, the third type, exhibit ores dominated by textures displaying medium to coarse-grained subhedral pyrite grains, and granuloblastic textures as the result of extensive hydrothermal recrystallization during the low-grade metamorphism.

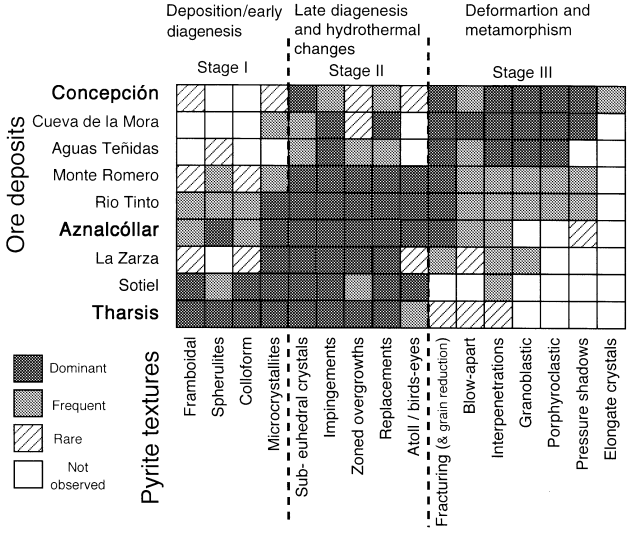

Fig. 4 Textural variation in massive pyrite ores (>95% pyrite). Main pyrite textures have been ordered approximately from primary to more evolved and metamorphic textures (*left* to *right*), whilst the studied ore deposits are organized taking into account their geographic location (approximately from NE to SW) concurrent with the increasing of metamorphic grade (Munhá 1983)

All the ores have undergone variable deformation and metamorphism which may be evidenced by a wide number of pressure solution textures such as interpenetrated grains, serrated, curved and irregular grain selvages, pressure shadows, and locally elongate crystals (stage III, Fig. 4). All these textures were probably produced at relative low temperature by fluid assisted diffussive mass transfer (McClay 1977; Marshall and Gilligan 1987). Because of the highly brittle nature of pyrite under relatively low temperature and pressure during regional metamorphism (Marshall and Gilligan 1987), massive IPB pyrite ores show diverse cataclastic textures such as blow-apart, cracking and fracture textures (cataclasis), porphyroclastic textures with remobilized chalcopyrite or galena infilling fractures. Elongated grains and oriented fabric may be the result of a combination of pressure solution, grain-boundary sliding and cataclastic flow. Such processes have been suggested to explain the macroscopic ductility of fine-grained pyrite ores in low-grade metamorphic environments (McClay and Ellis 1983; Craig and Vokes 1993). Sutured grain boundaries and very fine new grains of pyrite may have been developed by stress-induced grain boundary migration. Ductile sulphide grains such as chalcopyrite, sphalerite and galena normally display annealing twins, polygonal textures with triple junction angles approaching 120°, oriented overgrowths, and generalized recrystallization.

An important variety of textures, ranging from sedimentary to metamorphic textures, may be found as consequences of: (1) deposition; (2) diagenetic recrystallization and overgrowths during hydrothermal replacement; and (3) deformation and metamorphic recrystallization. The present-day textural variation in the ore sulphides among different deposits, and even over short distances in a single deposit or sample, is the result of the relative interplay of the four styles of deposition, as well as the relative proportions of ductile and brittle minerals in the mineral association. Most of the IPB ore deposits show pyrite exhibiting well-preserved primary depositional and diagenetic textures. In contrast pyrite mylonites, resulting from dynamic metamorphism in shear zones, which normally tend to obliterate existing features, are most frequent in the NE of the IPB (e.g. Concepción, Cueva de la Mora).

In short, textures are mostly controlled by the degree of replacement of original textures during hydrothermal stages, and/or deformation and metamorphism of the ores. Nevertheless, in the less deformed and recrystallized parts of the massive deposits, many textural features have been observed which are similar to those recorded for the undeformed Kuroko deposits (Yui and Ishitoya 1983; Eldridge et al. 1983). The distribution and relative importance of the preserved primary textures is consistent with the model of Ohmoto (1996), in which two main processes are established: (a) deposition and early diagenesis; and (b) recrystallization and ore re-

placement related to late diagenesis and hydrothermal alteration. Most of the primary ore deposition is assumed to have occurred during the waxing stage of hydrothermal activity at low temperature (< 150 °C), being later modified or altered by hotter hydrothermal fluids (≈200–350 °C). Subsequently, sulphides were weakly metamorphosed under conditions of very low to low degree metamorphism (Schermerhorn 1971; Munhá 1990; Fernández Caliani et al. 1994).

Sulphur isotopic study

Materials and analytical procedures

Sampling of massive and stockwork ores was facilitated from outcrop and drillcore. All samples were classified by their textural type and mineralogy, with a view to determine if there was any correlation between texture and $\delta^{34}S$. Sulphur isotope analyses were carried out by two methods at the SURRC, Glasgow (Scotland, UK): (1) sulphides extracted by hand-drilling of polished hand specimens and blocks using conventional procedures (after Robinson and Kusakabe 1975); and (2) performed in situ via laser extraction (Fallick et al. 1992), on fine-grained sulphide intergrowths and coarse grain crystals, in well characterized polished blocks. The conventionally analyzed sulphides were generally concentrates with varying proportions of pyrite, sphalerite, chalcopyrite and galena.

In all cases, the composition of the conventionally processed mixtures was controlled by microscopic examination. By contrast, laser analyses were performed on monomineralic sulphides of varying morphology and grain size (e.g. framboids, colloform structures, spherulites, cubic aggregates, zoned overgrowths, and recrystallized coarse grains). Typically, laser analyses were carried out over an area around 300 μm by 300 μm for sulphide minerals. All results are reported in delta notation, as per mil (‰) variations from the Cañon Diablo troilite (CDT) standard. Error of reproducibility, based on repeated analyses of internal and international standards was better than ± 0.3‰ for both techniques.

Sulphur isotope data

One hundred and thirteen new $\delta^{34}S$ analyses (conventional and laser) are listed in Table 3, mainly from the Tharsis ($n = 27$), Aznalcóllar ($n = 28$), and Concepción ($n = 23$) mines. In addition, 35 analyses from the more intensely deformed and metamorphosed deposits in the NE part of the IPB – Aguas Teñidas mine ($n = 16$), Cueva de la Mora ($n = 6$) and Monte Romero ($n = 11$) – and the barites ($n = 2$; Sierrecilla and San Platón), have also been performed. The sulphur isotopic statistics and the main mineralogical and textural features are listed in Table 4 and plotted in Fig. 5 as histograms. These data confirm, as noted already, the general sulphur isotopic distribution described in the literature (see also Fig. 2 and Table 1).

In the *Tharsis Mine*, where colloform, framboidal and other primary textures are dominant, most of the massive ores have mainly negative $\delta^{34}S$ values ranging from −26.5‰ to +2.2‰ with a mean of −5.6‰. In contrast, stringer sulphides have $\delta^{34}S$ close to 0‰. In the *Aznalcóllar Mine,* where replacement and recrystallization textures are more frequent, the $\delta^{34}S$ range is −8.1 to +5.6‰ with a mean of −0.8‰ the isotopic signatures of primary ores, displaying less evolved textures, are shifted to more negative values. In *Concepción Mine*, in which primary textures are less well preserved, the isotopic range is from −15.1 to +10.1‰ with an average value of +2.8‰ (median of +5.3‰). It is interesting to note that all three deposits show a few analysis shifted to the very negative extreme values (see Fig. 5). The $\delta^{34}S$ range for massive sulphides from Cueva de la Mora and Monte Romero deposits is +2.5 to +9.0‰ (averages in +5.2 and +6.6‰, respectively), whereas in the Aguas Teñidas deposit, the $\delta^{34}S$ average for massive sulphides is +0.3‰.

Where available for sampling, the stockwork ores almost always display the most positive values (Table 3), with average of +0.2‰ (Tharsis), +2.1‰ (Aznalcóllar), and +5.8‰ (Concepción). Similar results to Concepción were reported from the Rio Tinto mine stockwork, with average $\delta^{34}S$ reported between +5 and +11‰ (Eastoe et al. 1986) and +9‰ (Mitsuno et al. 1988). Likewise, the reported values for the Tharsis stockwork, ranging between −4.5 and +1.9‰ (Kase et al. 1990; Tornos et al. 1998), match with our results (+0.2‰).

Isotope sulphur ratios for two barites from San Platón (a small orebody close to Concepción) and Sierrecilla (located about 15 km NW from Tharsis) were also determined. Their respective $\delta^{34}S$ values of +21.5 and +19.5‰ are quite similar to the highest values (+22‰) from barites reported by Mitsuno et al. (1988), Eastoe et al. (1986), and Yamamoto et al. (1993) for San Telmo and Rio Tinto deposits; the $\delta^{34}S$ values of barites from the IPB (Table 1) range from +15 to +24‰ (average of +17.8‰).

A strong relationship between the measured $\delta^{34}S$ (mostly by laser) and the different textures displayed by these minerals is observed (Fig. 6). Primary and less evolved textures such as framboidal, spherulitic, unrecrystallized colloform overgrowths, and other fine-grained sulphide crystals show negative average ($\delta^{34}S$ values between −15.1 to +2.2‰). The more evolved textures, such as euhedral to subhedral crystals, as well as replacement textures and coarse-grained crystals, exhibit more positive values (up to +10.2‰). Transitional textures, being the product of variable replacement and recrystallization effects, are reflected by intermediate $\delta^{34}S$ between the two end-member groups of morphologies.

A comparison of the results performed by conventional and laser methods reveals that there is much more variation in $\delta^{34}S$ when the in situ analysis are considered. Data from complex textures, involving various depositional styles, display wide isotopic variation. There is a relationship between the conventional results and the "average" of the more heterogeneous laser data coming from the same sample, showing that conventional analysis maintain their efficacy in general isotopic studies. However, when heterogeneous and fine-grained sulphides are concerned, the in situ analysis confers obvious advantages.

Table 3 New sulphur isotope data for ore minerals from the studied IPB deposits

Sample	Minerals	$\delta^{34}S‰$	Ore type	Description	Method
THARSIS					
TH-6	Gn (+Cp)	− 8.3	Massive	Fracture filled up in massive pyrite	C
TH-7	Py (+Cp)	− 1.3	Massive	Massive Py + minor Cp	C
TH-9	Cp-Sp-Gn	− 5.4	Massive	Thin bed in the massive body	C
TH-9	Cp	− 5.3	Massive	Fracture filled up in massive pyrite	C
TH-co.	Py (+Cp)	− 3.3	Massive	Fine-grained Py + Cp	C
TH-co./2	Py (+Cp)	− 7.9	Massive	Fine-grained Py + Cp	C
TH-d.	Py (+Cp)	− 7.3	Massive	Fine-grained Py + minor Cp	C
TH-2	Py	− 6.1	Banded	Colloform	L
TH-2	Py	−12.9	Banded	Framboidal	L
TH-2	Py	−13.1	Banded	Framboidal	L
TH-2	Py	− 9.1	Banded	Idiomorphic crystal	L
TH-2	Sp-Gn	− 6.9	Banded	Thin massive band	L
TH-10	Py	− 2.7	Massive	Idiomorphic crystal	L
TH-10	Py	+ 1.5	Massive	Idiomorphic crystal	L
TH-10	Py	− 2.9	Massive	Idiomorphic crystal	L
TH-10	Sp	−26.5	Massive	Massive. fine-grained	L
TH-10	Sp	−20.1	Massive	Massive. fine-grained	L
TH-1	Py	+ 2.2	Banded	Colloform	L
TH-1	Py	− 1.3	Banded	Very fine-grained. (melnikovite)	L
TH-1	Py	− 0.9	Banded	Colloform	L
TH-1	Py	+ 2.1	Banded	Very fine-grained. (melnikovite)	L
TH-1	Py	− 1.7	Banded	Colloform	L
MUR-N.	Py	− 3.5	Nodule	Diagenetic nodule in shale	C
TH-Stk	Py	+ 0.2	Stringer	Py dissemination in stockwork ore	C
TH-Stk	Py	+ 0.4	Stringer	Euhedral crystal in stockwork vein	L
TH-Stk	Py	+ 0.4	Stringer	Euhedral crystal in stockwork vein	L
TH-Stk	Py	+ 0.6	Stringer	Euhedral crystal in stockwork vein	L
AZNALCOLLAR					
A15/280	Py	− 1.1	Banded	Framboidal	L
A15/280	Py	− 0.4	Banded	Framboidal	L
A15/280	Py	− 0.3	Banded	Idiomorphic crystal	L
A15/280	Py	+ 0.8	Banded	Idiomorphic crystal	L
A15/280	Py	− 0.3	Banded	Colloform	L
A15/280	Sp	− 1.4	Banded	Thin massive band	L
A15/280	Sp	− 2.5	Banded	Thin massive band	L
BRT-61	Cp	− 1.1	Massive	Massive, fine-grained	L
BRT-61	Cp	− 1.6	Massive	Massive, fine-grained	L
G4-LF1″	Py	− 8.1	Massive	Framboidal	L
G4-LF1″	Sp	+ 0.5	Massive	Massive, fine-grained	L
G4-LF1″	Gn	+ 2.9	Massive	Massive, fine-grained	L
G4-LF1″	Py	+ 2.4	Massive	Idiomorphic crystal	L
G4-LF1″	Py	− 6.1	Massive	Framboidal	L
G4-LF1″	Py	+ 0.2	Massive	Colloform	L
458–492	Py (+Cp-Gn)	− 2.1	Massive	Thin bed in the massive body	C
6-PA5	Cp	− 2.2	Massive	Fracture filled up in massive pyrite	C
BRT-61	Cp	− 1.8	Massive	Fracture filled up in massive pyrite	C
BRT-61	Py (+Cp-Gn)	− 2.5	Massive	Large pyritic massive area	C
G1-LF-1	Py (+Cp-Gn)	− 0.3	Massive	Thin pyritic massive bed	C
TLF-11	Gn (+Py-Cp)	− 3.4	Massive	Fracture filled up in massive pyrite	C
TLF-11	Gn (+Py-Cp)	− 3.3	Massive	Fracture filled up in massive pyrite	C
TLF-11	Py (+Cp-Gn)	− 0.8	Massive	Large pyritic massive area	C
FR-PyD	Py	+ 5.6	Banded	Disseminated Py in shale	C
TLF-24	Py	+ 0.0	Massive	Mainly sub-automorph	C
G1-LF-1	Sp	+ 0.0	Banded	Diseminated in black shales	C
A34-400	Py	+ 3.2	Stringer	Coarse grained automorph pyrite	C
TLF-2	Py	+ 1.0	Stringer	Medium grained pyrite	C
CONCEPCIÓN					
CO-1	Py (+Cp)	+ 5.3	Massive	Massive Py + minor Cp	C
CO-20	Py (+Cp)	+ 6.2	Stringer	Py dissemination in host rock	C
CO-8	Py (+Cp-Sp)	+ 4.1	Massive	Massive Py + minor sulphides	C
CO-95.M	Py (+Cp-Sp)	+ 5.9	Massive	Massive Py + minor sulphides	C
CO-95.11	Py	+ 7.3	Massive	Idiomorphic crystal	L
CO-95.11	Py	+ 5.1	Massive	Elongated recrystallized grains	L
CO-95.11	Sp	+ 6.2	Massive	Massive. fine-grained	L
CO-95.11	Cp	+ 4.3	Massive	Massive. fine-grained	L
CO(g)-3	Py	− 8.5	Banded	Framboidal	L
CO(g)-3	Py	− 9.7	Banded	Framboidal	L

Table 3 (Continued)

Sample	Minerals	$\delta^{34}S‰$	Ore type	Description	Method
CO(g)-3	Py	−15.1	Banded	Framboidal	L
CO(g)-3	Py	+ 6.1	Banded	Brecciated. coarse-grained	L
CO(g)-3	Sp	− 1.8	Banded	Thin massive band	L
CO(g)-1	Py	− 9.1	Banded	Framboidal	L
CO(g)-1	Sp	− 0.2	Banded	Thin massive band	L
CO(g)-1	Py	+ 5.2	Banded	Massive. syneresis cracks	L
CO(g)-1	Py	− 9.3	Banded	Framboidal	L
CO-8	Py	+ 7.7	Massive	Massive, coarse-grained	L
CO-14	Py (+Cp)	+ 4.1	Stringer	Py dissemination in stockwork ore	C
CO-95.Stk	Py (+Cp)	+ 8.1	Stringer	Py dissemination in stockwork ore	C
CO-6	Py (+Cp)	+ 5.6	Stringer	Py dissemination in stockwork ore	C
CO-95.Stk	Py	+ 10.2	Stringer	Euhedral crystal in stockwork vein	L
CO-95.Stk	Py	+ 9.8	Stringer	Euhedral crystal in stockwork vein	L
AGUAS TEÑIDAS					
AT-11	Py-Cp-Sp-Gn-Te	+ 1.3	Banded	Fine-grained massive bands	C
AT-12	Py-Cp-Sp-Gn-Te	− 5.7	Banded	Fine-grained massive bands	C
AT-12	Py-Cp-Sp-Gn-Te	− 5.1	Banded	Fine-grained massive bands	C
AT-4	Py-Cp-Sp-Gn-Te	+ 3.6	Banded	Fine-grained massive bands	C
AT-9	Py-Cp-Sp-Gn-Te	+ 0.3	Banded	Fine-grained massive bands	C
AT-95.1	Py-Cp-Sp-Gn-Te	+ 1.4	Banded	Fine-grained massive bands	C
AT-11	Py-Cp-Sp-Gn-Te	+ 1.6	Banded	Fine-grained massive bands	C
AT-5″	Py-Cp-Sp-Gn	+ 2.6	Banded	Fine-grained massive bands	C
AT-8	Py-Cp-Sp-Gn	− 0.2	Banded	Fine-grained massive bands	C
AT-8	Py	+ 3.2	Banded	Idiomorphic crystal	L
AT-8	Sp	+ 1.6	Banded	Massive, coarse-grained	L
AT-11	Py	+ 3.2	Banded	Idiomorphic crystal	L
AT-11	Sp-Gn	+ 0.8	Banded	Thin massive band	L
AT-12	Py	+ 0.1	Banded	Idiomorphic crystal	L
AT-12	Py	+ 0.5	Banded	Idiomorphic crystal	L
AT-12	Sp-Gn	− 4.8	Banded	Thin massive band	L
CUEVA DE LA MORA					
CM-1	Sp-Cp	+2.9	Banded	Coarse-grained sulphide lens	C
CM-10	Sp-Gn-Te-Py	+5.5	Banded	Coarse-grained sulphide lens	C
CM-9	Py (Cp)	+7.1	Stringer	Py dissemination in host rock	C
CM-10	Py	+6.9	Banded	Idiomorphic crystal	L
CM-10	Sp	+6.2	Banded	Thin massive band	L
CM-10	Te	+2.5	Banded	Thin massive band	L
MONTE ROMERO					
MR-5	Py-Cp-As-Sp-Gn	+3.3	Banded	Fine-grained massive bands	C
MR-6	Py-Cp-As-Sp-Gn	+6.5	Banded	Fine-grained massive bands	C
MR-95.1	Cp-Gn + Sp + Gn	+5.5	Banded	Fine-grained massive bands	C
MR-95.1	Cp (+Gn)	+5.3	Banded	Fracture filled up in massive pyrite	C
MR-95.1	Gn-Cp (+Sp-Py)	+5.6	Banded	Fine-grained massive bands	C
MR-6	Py	+8.5	Banded	Idiomorphic crystals	L
MR-6	Py	+9.1	Banded	Idiomorphic crystals	L
MR-6	Sp	+8.1	Banded	Massive, coarse-grained	L
MR-6	Cp	+6.3	Banded	Massive, coarse-grained	L
MR-6	Cp	+6.7	Banded	Massive, coarse-grained	L
MR-6	Te	+7.1	Banded	Thin massive band	L
BARITES					
Bar-SanP	Ba	+21.5	Massive	Large euhedral crystal	C
SR-1	Ba	+19.5	Massive	Stratiform massive barite	C

Abreviations: Py-pyrite, Sp-sphalerite, Gn-galena, Cp-chalcopyrite, Te-tetrahedrite, As-arsenopyrite, Ba-barite
Analytical method: L-laser analyses, C-conventional analyses

Discussion

A notable geochemical characteristic of the volcanic-hosted massive sulphide deposits of the IPB is the remarkable variation of their sulphur isotopic composition among different ore deposits (values fall in a broad range from −26‰ to +10‰), and even within each deposit and ore facies. This feature contrasts with the majority of Kuroko deposits which generally exhibit a relative narrow scatter of $\delta^{34}S$ values, mostly between 0 and +8‰ (Ohmoto and Rye 1979; Ohmoto 1996), suggesting a relative homogeneity in fluid sulphur composition and similar physico-chemical conditions during ore forming processes. In the same way, recent studies on the East Pacific Rise (Bluth and Ohmoto 1988;

Table 4 Summary statistics of sulphur isotope compositions in ‰ $\delta^{34}S$ from the selected IPB sulphur massive deposits (conventional plus laser) and principal textural types (only laser analysis)

	Number	Mean	Median	SD	Minimum	Maximum	IntQRange
Massive deposits (conventional + laser)							
Ore deposits							
Aguas Teñidas	16	+0.3	+1.1	2.9	−5.6	+3.6	2.1
Aznalcollar	28	−0.8	−0.6	2.7	−8.1	+5.6	2.5
Concepción	23	+2.8	+5.3	6.8	−15.1	+10.1	6.2
Cueva de la Mora	6	+5.2	+5.8	2.0	+2.5	+7.1	3.9
Monte Romero	11	+6.6	+6.5	1.6	+3.3	+9.0	2.3
Tharsis	27	−5.6	−3.5	6.9	−26.5	+2.2	8.0
Textures (laser only)							
Texture type							
1. Framboidal/spherulitic	8	−7.6	−8.3	5.1	−15.1	−0.4	7.4
2. Colloform	12	−2.5	−1.1	5.3	−12.8	+2.2	7.8
3. Subhedral crystals	20	+1.8	+1.2	4.7	-9.0	+9.0	6.3
4. Replacement/recrys.	19	+2.7	+3.2	4.3	-6.9	+8.1	7.9
5. Coarse grained	11	+3.9	+3.2	3.9	+0.2	+10.2	6.9

IntQRange, interquartile range

Graham et al. 1988; Hannington and Scott 1988), and in Deep Sea Drilling Project (Herzig 1997; Petersen et al. 1997), show the existence of a continuous interaction between pore fluids (former seawater) and volcanic rocks, during diagenesis and hydrothermal replacements, giving sulphides with $\delta^{34}S$ ranging from +4 to +10‰ (Zierenberg and Shanks 1988; Bluth and Ohmoto 1988; Petersen et al. 1997). Only one modern ridge hydrothermal site has so far produced significantly negative $\delta^{34}S$: the Lau Basin (Herzig et al. 1997). Here, pyrite was noted with $\delta^{34}S$ down to −7.7‰, which was attributed to disproportionation of magmatic volatiles, highlighted by the presence of texturally and isotopically distinct alunite (unique to this site; Herzig et al. 1997).

As stated already, our $\delta^{34}S$ data set can be broken down by textural association. There are clearly two end-

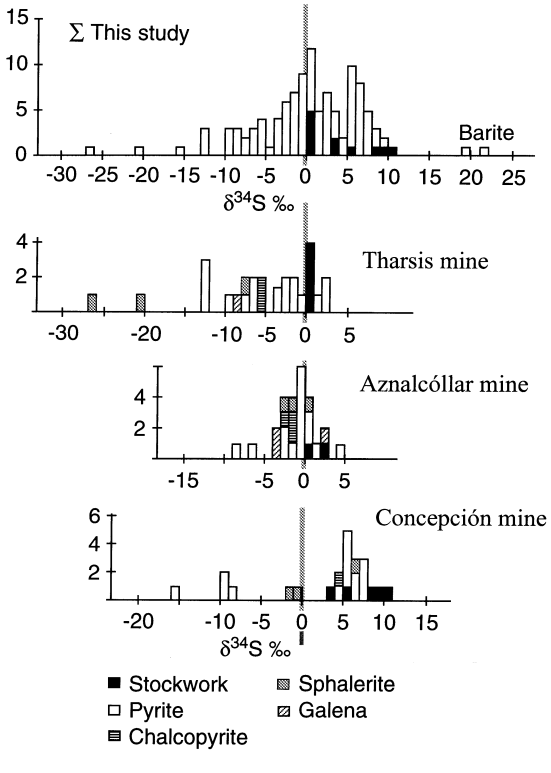

Fig. 5 Histograms of obtained $\delta^{34}S$ data for the main sulphides from Tharsis, Aznalcóllar and Concepción deposits (analysis performed by laser and conventional techniques). The plot shows that the pattern of the total sulphur isotope compositions found in this study is similar to the summary of the $\delta^{34}S$ data for the whole Iberian Pyrite Belt (compare the *uppermost histogram* with Fig. 2)

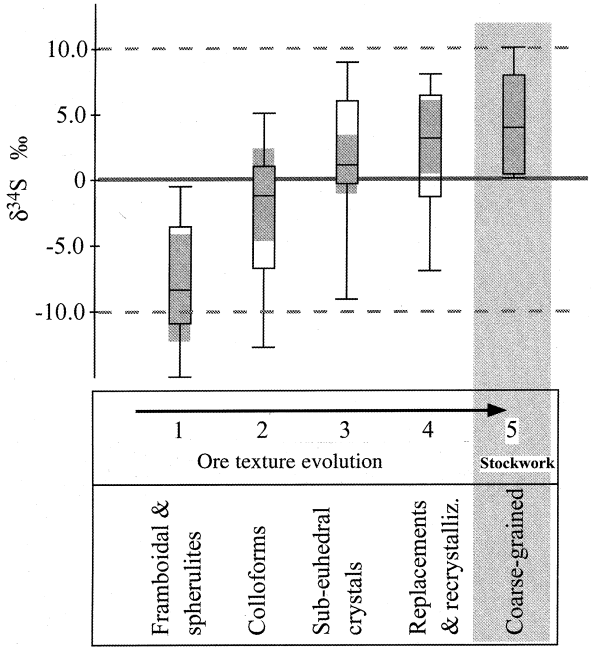

Fig. 6 Plot of the $\delta^{34}S$ values for pyrite from different textural types showing a close relationship between $\delta^{34}S$ and textural style. *Boxplots* indicate the range and the increasing mean of $\delta^{34}S$ composition of early-primary pyrites (*1* and *2* texture types) to secondary (*3* and *4*), and hydrothermal (*5*) pyrites

members. The first, and most obvious is the low $\delta^{34}S$ associated with the less evolved, early diagenetic textures. The second is the high $\delta^{34}S$ component seen in the stockwork ores. In both cases, pristine materials preserve the original $\delta^{34}S$. The range of $\delta^{34}S$ recorded by these materials spans the entire range we have measured, and cannot be explained by comparison with accepted processes proposed to explain $\delta^{34}S$ in modern ridges, or in Kuroko deposits.

The source for the rare sulphates present in the IPB is relatively straightforward. The range and mean of the isotopic data (+15‰ to +24‰; +18‰ respectively) fall within the range accepted for Lower Carboniferous seawater sulphate, therefore it is likely that exhaled Ba combined directly with seawater sulphate at the time of barite precipitation. Typically, bacterial reduction of modern seawater sulphate (an extremely common process in the absence of dissolved oxygen in the marine environment) results in sulphide with a $\delta^{34}S$ around 40 ± 20‰ lower than the starting sulphate (Goldhaber and Kaplan 1974; Ohmoto 1986). In the Lower Carboniferous Irish Zn + Pb + Ba deposits (penecontemporaneous with the IPB deposits), the fractionation is typically 35 ± 15‰ (Boyce and Fallick 1995). Applying this fractionation to the IPB deposits would result in a range of sulphide with $\delta^{34}S$ between −2‰ and −32‰, with the modern fractionation extending this range towards even higher or lower values. Examining our data, the range of $\delta^{34}S$ for sulphides with primary diagenetic textures (labelled S on Fig. 7) is dominantly negative (between −26‰ and +3‰, with median around −2.5‰). Thus, these data are consistent with a bacteriogenic derivation of this sulphide.

The hydrothermal component, exemplified by sulphides in the stockwork feeder zones, display a positive range of $\delta^{34}S$ with a mode around + 6‰ (between +2‰ and +10.2‰, with median of +5.6‰). In these high temperature zones near the seafloor (200–350 °C: Toscano et al. 1993; 1997; Almodóvar et al. 1998), there is little evidence for oxidizing conditions, witnessed by the absence of barite and haematite, and the notable presence of pyrrhotite (especially abundant at Sotiel) or magnetite (e.g. Concepción). Thus, the solutions were consistently reducing, in which case the $\delta^{34}S$ of precipitated sulphide minerals closely reflects the $\delta^{34}S$ of the hydrothermal solutions (Ohmoto and Rye 1979). Experimental evidence indicates that sulphate is reduced in high temperature hydrothermal systems interacting with volcanic rocks by oxidation of Fe^{2+} (Ohmoto and Rye 1979). This results in a fractionation between 0‰ and 25‰ lower than the starting sulphate, depending on the degree of reduction which governs the SO_4/H_2S ratio (Rye and Ohmoto 1974). Such a process has been invoked to account for the spread to positive values of $\delta^{34}S$ in modern vent sulphides (e.g. Bluth and Ohmoto 1988; Petersen et al. 1997).

We suggest a similar process was operating in the hydrothermal systems responsible for the deposition of the IPB deposits. It is noted that most of the intermediate textures (in general, coarser) have $\delta^{34}S$ with median around +1‰ and +3‰ (3 and 4 ore texture types, respectively in Fig. 6), which is significantly heavier than the primary sulphides, and overlaps with the feeder sulphide isotopic range. This indicates that the dominant component in these sulphides was also hydrothermal, that is, derived from reduction of seawater sulphate in the hydrothermal system. This is true of most of these sulphides even where they occur away from known stockwork zones. Evidence of both primary and replacement sulphur components can be documented by the existence of scattered remains of framboidal and fine grains of pyrite, within recrystallized massive pyrite from Concepción mine (see Fig. 3B), displaying $\delta^{34}S$ values of −9.3 and +5.2‰, respectively. Such observed dramatic variation of up to 15‰ occurs among pyrites separates smaller than 200 μm in size from a single rock specimen. This suggests that the process responsible for the intermediate textures overprinted the early textures, and deposited new sulphide during the evolution of the hydrothermal system. The low-grade metamorphism (greenschist facies) does not appear to have significantly altered the $\delta^{34}S$ of sulphides. It is generally accepted that metamorphism tends to homogenize and reduce the range of $\delta^{34}S$ in a deposit (Sangster 1971), since preservation of the primary isotope fractionation patterns is the dominant rule (Cook and Hoefs 1997). However, our documented variation of $\delta^{34}S$ values among sulphide grains from the same rock specimen demonstrates

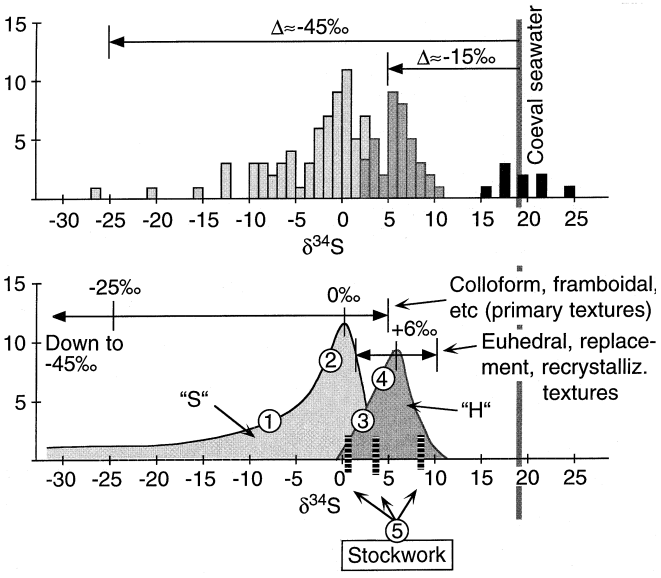

Fig. 7 Summary histogram compared with a simplified schematic representation of the data for the sulphur isotope composition of sulphide minerals from the studied orebodies. This plot illustrate the consequences of the isotope-texture style dependence by heuristically divided $\delta^{34}S$ histogram into two contributing components: "*H*" and "*S*" labels are the signatures of the ores formed by inorganic reduction (hydrothermal fluids) and by bacteriogenic reduction of seawater sulphate, respectively. *1*, *2*, *3*, and *4* represent average compositions of the main ore texture evolution stages (see Fig. 6 and explanation in the text). Some additional barite data (*black bars*) are from Eastoe et al. (1986) and Mitsuno et al. (1988)

that very limited homogenization took place during regional metamorphism.

Like many previous authors (Lécolle 1977; Routhier et al. 1978; Eastoe et al. 1986; Mitsuno et al. 1988; Kase et al. 1990; Yamamoto et al. 1993; Sáez et al. in press), we favour a dual source of sulphur for the deposits. Overall, it appears that there was a mixed sulphide source in the IPB deposits: one, a bacteriogenic component found at or near the seafloor, and the other, a hydrothermal component created by the chemical reduction of seawater in the hydrothermal system, and carried towards the seafloor with the leached metals. Nevertheless, for this last source some minor contribution from magmatic sulphur (leached from underlying volcanic rocks) should be also considered. It is therefore possible to account for the distinct isotopic variations between deposits, by assuming some variation in the relative contributions of the two reservoirs, most likely caused by differences in the local geological environment during deposition. It is thus possible that the regional trend towards higher $\delta^{34}S$ in the NE (Figs. 1 and 2) may indicate that the systems in these areas were dominated more by the hydrothermal component than those towards the SW. However, our detailed textural and laser analyses indicate that both sulphur sources were present in all the deposits studied. Finally, given this dual source model, quite unlike modern vent systems and most ancient VMS deposits, together with the frequently intimate spatial relationship between the sulphide ores, volcanic rocks and interlayered black shales and other reduced sediments, we suggest that the IPB deposits could be considered as a distinct type, intermediate between clastic sediment-hosted (SEDEX) massive deposits (Sáez et al. in press), and more typical VMS deposits in a dominantly volcanic environment.

Conclusions

1. The detailed petrographic and in situ laser sulphur isotope analyses have revealed a close correlation between different textural styles and $\delta^{34}S$.

2. Primary sulphide growth textures (e.g. framboids, colloform growths, spheroids, shrinkage or syneresis cracks, and microcrystallites) have dominantly low $\delta^{34}S$ (between $-26‰$ and $+3‰$), whereas feeder stockwork ores have dominantly high $\delta^{34}S$ (between $0‰$ and $+10‰$).

3. Intermediate textures (e.g. zoned overgrowths, subhedral to euhedral crystals, and impingement overgrowths) have an intermediate $\delta^{34}S$ range, although mainly towards higher $\delta^{34}S$ (averages between $+1‰$ and $+3‰$).

4. The data are consistent with a dual source of sulphide sulphur. The first, represented mainly in the primary diagenetic stratiform zones (but also seen in the intermediate textures), is from the bacterial reduction of coeval seawater sulphate. The second source, evidenced in the stockwork and most of the intermediate textures, is a hydrothermal source derived from the reduction of coeval seawater sulphate in the convective systems. The spread of data relates to the extent of the reduction, which controls the SO_4:H_2S ratio in the solutions. In both cases the systems were reduced and dominated by sulphide. The variation in intra-deposit spread of $\delta^{34}S$ across the province reflects a variation in the relative input from these reservoirs, most likely controlled by the geological conditions prevailing at each deposit. Rare barite in the IPB deposits has quite homogeneous $\delta^{34}S$ around $+18‰$, which is consistent with direct derivation from Lower Carboniferous seawater sulphate.

5. There is a distinct geographical variation in textural dominance and corresponding $\delta^{34}S$ in the IPB deposits, which suggests that deposits in the NE have a stronger component of the hydrothermal source than deposits in the SW, which have more bacteriogenic sulphur. However, both sulphide sources are seen across the province.

6. Noting that the IPB deposits have a distinct isotopic signature compared to most VMS deposits, and given the strong association of volcanics and reduced sediments, we suggest that the IPB deposits could be considered as a new type of the large group of volcanic associated massive sulphide deposits, exhibiting a number of features more typical of the clastic sediment hosted base metal deposits.

7. Our study highlights the strength of using in situ laser sulphur isotope analyses on paragenetically controlled samples in unravelling the origin of sulphide ore deposits.

Acknowledgements Sampling ores and access to mines was made possible by Navan Resources, S.A., Boliden-Apirsa, Minas de Rio Tinto, S.A.L., and Minas de Tharsis. We gratefully acknowledge the Universidad del País Vasco (project UPV 130.310-EB037/96), Gobierno Vasco (JSE was funded for a PhD grant) and Grupo RNM 198 del Plan Andaluz de Investigación (Junta de Andalucía) and DGICYT project AMB94-0243 for financial support. The Isotope Geoscience Unit at SURRC is supported by NERC and the consortium of Scottish Universities, AJB is funded at SURRC through the NERC Isotope Community Support Facility. The authors would also like to thank Nigel Cook and Victor A. Melezhik for their useful comments which significantly improved the manuscript.

References

Arnold M, Bernard AJ, Soler E (1977) Premier apport de la géochimie des isotopes du soufre à la compréhension de la genèse des minéralisations pyriteuses de la Province de Huelva (Espagne). Mineral Deposita 12: 197–218

Almodóvar GR, Sáez R (1992) Los yacimientos de sulfuros masivos de la Faja Pirítica Sur–Ibérica In: García Guinea J, Martínez Frías J (eds) Recursos Minerales de España. C.S.I.C., Madrid, pp 1309–1324

Almodóvar G, Sáez R, Toscano M, Pascual E (1995) Co, Ni, and "inmobile" element behaviour in ancient hydrotermal systems, Aznalcóllar, Iberian Pyrite Belt, Spain. In: Pasava, Kríbev, Zák (eds) Mineral deposits: from their origin to their environmental impact. Balkema, Rotterdam, pp 217–219

Almodóvar G, Sáez R, Pons JM, Maestre A,Toscano M, Pascual E (1998) Geology and genesis of the Aznalcóllar massive sulphide

deposits, Iberian Pyrite Belt, Spain. Mineralium Deposita 33: 111–136
Barriga FJAS (1990) Metallogenesis in the Iberian Pyrite Belt. In: Dallmeyer RD, Martínez-García E (eds). Pre-Mesozoic geology of Iberia. Springer Verlag, Berlin Heidelberg New York, pp 369–379
Bluth GJ, Ohmoto H (1988) Sulphide-sulphate chimneys on the East Pacific Rise, 11° and 13°N latitudes. Part II: sulphur isotopes. Can Mineral 26: 505–516
Boyce AJ, Fallick AE (1995). Stable and radiogenic isotope constraints on genetic models for the Lower Carboniferous carbonate-hosted Zn + Pb + Ba deposits in Ireland. Extended abstract in Models for Carbonate-hosted Base-Metal Deposits, Irish Association for Economic Geology Dublin, pp 49–53
Cagatay MN, Eastoe CJ, (1995) A sulfur isotope study of volcanogenic massive sulfide deposits of the Eastern Black Sea province, Turkey. Mineralium Deposita 30: 55–66
Carvalho D, Correia HAC, Inverno CMC (1976) Livro guia das excursoes geologicas na Faixa Piritosa Iberica. Comun Serv Geol Port 60: 271–315
Cook NJ, Hoefs J (1997) Sulphur isotope characteristics of metamorphosed Cu-(Zn) volcanogenic massive sulphide deposits in the Norwegian Caledonides. Chem Geol 135: 307–324
Cox SF (1987) Flow mechanisms in sulphide minerals. Ore Geol Rev 2: 133–171
Craig JR, Vokes FM (1993) The metamorphism of pyrite and pyritic ores: an overview. Mineral Mag 57: 3–18
Eastoe CJ, Solomon M, García Palomero F (1986) A sulfur isotope study of the massive and stockwork pyrite deposits at Rio Tinto, Spain Trans Inst Min Metall 95: B201–207
Eldridge CS, Barton PB, Ohmoto H (1983) In: Ohmoto H, Skinner BJ (eds) The Kuroko and related volcanogenic massive sulphide deposits. Econ Geol Monogr 5: 241–281
Eldridge CS, Compston W, Williams IS, Both RA, Walshe JL, Ohmoto H (1988) Sulfur isotope variability in sediment-hosted massive sulphide deposits as determined using the ion microprobe SHRIMP: I. An example from the Rammelsberg orebody. Econ Geol 83: 443–449
Eldridge CS, Williams IS, Walshe JL (1993) Sulfur isotope variability in sediment-hosted massive sulfide deposits as determined using the Ion Microprobe SHRIMP: II. A Study of the HYC. Deposit at McArthur River, Northern Territory, Australia. Econ Geol 88: 1–26
Fallick AE, McConville P, Boyce AJ, Burgess R, Kelley SP (1992) Laser microprobe stable measurements on geological materials: some experimental considerations (with special reference to $\delta^{34}S$ in sulphides). Chem Geol 101: 53–61
Fernández Caliani JC, Mesa JM, Galán E (1994) Características del metamorfismo de grado bajo a muy bajo en la parte meridional de la Faja Pirítica (Zona Sur Portuguesa). Bol Geol Min 105–2: 213–220
García de Miguel JM (1990) Mineralogía, paragénesis y sucesión de los sulfuros masivos de la Faja Pirítica en el suroeste de la Península Ibérica. Bol Geol Miner 101: 73–105
Goldhaber MB, Kaplan IR (1974) The sedimentary sulfur cycle. In: Goldberg EB (ed) The sea, vol IV. Wiley, New York
Graham UM, Bluth GJ, Ohmoto H (1988) Sulphide-sulphate chimneys on the East Pacific Rise, 11° and 13°N latitudes. part I: mineralogy and paragenesis. Can Mineral 26–3: 487–504
Hannington MD, Scott SD (1988) Mineralogy and geochemistry of a hydrothermal silica-sulphide-sulphate spire in the caldera of Axial Seamount, Juan de Fuca Ridge. Can Mineral 26–3: 603–626
Herzig PM (1997) Present-day submarine hydrothermal systems: an up-date. Proc Abstrs SEG Field Conf 1997, Lisbon, Portugal, p 23
Herzig PM, Petersen S, Tichomirowa M, Hannington MD, Arribas A (1997) Unusual sulfur isotopic composition of volcanic-hosted massive sulfide deposits at the modern seafloor: TAG hydrothermal mound (MAR) and Lau back-arc (SW-Pacific). In: Papunen H (ed) 'Mineral deposits research and exploration. Where do they meet.?' Turku, Finland, pp 363–366
Hutchinson CS (1983) Economic deposits and their tectonic setting. MacMillan Press, London, 365 pp
Kase K, Yamamoto M, Nakamura T, Mitsuno C (1990) Ore mineralogy and sulfur isotope study of the massive sulphide deposit of Filon Norte, Tharsis Mine, Spain. Mineral Deposita 25: 289–296
Kelley SP, Fallick AE (1990) High precision spatially resolved analysis of $\delta^{34}S$ in sulphides using a laser extraction technique. Geochimi Cosmochim Acta 54: 883–888
Lianxing G, McClay KR (1992) Pyrite deformation in stratiform lead-zinc deposits of the Canadian Cordillera. Mineralium Deposita 27: 169–181
Lécolle M (1977) La ceinture sud–ibérique: un exemple de province à amas sulfurés volcano– sedimentaires. Thése, Université de P. et M. Curie, Paris, 613 pp
Marcoux E, Moelo Y, Leistel JM (1996) Bismuth and cobalt minerals as indicators of stringer zones to massive sulphide deposits, Iberian Pyrite Belt. Mineralium Deposita 31: 1–26
Marshall B, Gilligan LB (1987) An introduction to remobilization: Information from orebody geometry and experimental considerations. Ore Geol Rev 2: 87–131
McClay KR (1977) Pressure solution and Coble creep in rocks and minerals: a review. J Geol Soc London 134: 57–70
McClay KR, Ellis PG (1983) Deformation and recrystallization of pyrite. Mineral Mag 47: 527–538
McClay KR (1991) Deformation of stratiform Zn-Pb (-barite) deposits in the northern Canadian Cordillera. Ore Geol Rev 4: 435–462
Mitsuno C, Nakamura T, Yamamoto M, Kase K, Oho M, Suzuki S, Thadeu D, Carvalho D, Arribas A (1988) Geological studies of the "Iberian Pyrite Belt" with special reference to its genetical correlation of the Yanahara ore deposits and others in the inner zone of southwest Japan. University of Okayama, Japan, 300 pp
Moreno C, Sierra S, Sáez R (1996) Catastrophism evidence in the Famennian–Dinantian limit of the Iberian Pyrite Belt. In: Strogen P, Sommerville ID, Jones GL (eds) European Dinantian Environments. Geol Soc London Spec Publ 107: 153–162
Munhá J (1983) Hercynian magmatism in the Iberian Pyrite Belt. Mem Serv Geol Port 29: 39–81
Munhá J (1990) Metamorphic evolution of the South Portuguese/Pulo do Lobo Zone. In: Dallmeyer RD, Marínez García E (eds) Pre-Mesozoic geology of Iberia. Springer-Verlag, Berlin Heidelberg New York, pp 363–368
Munhá J, Kerrich R (1980) Sea water–basalt interaction in spilites from the Iberian Pyrite Belt. Contrib Mineral Petrol 73: 191–200
Ohmoto H, Rye RO (1979) Isotopes of sufur and carbon. In: Barnes HL (ed) Geochemistry of hydrothermal ore deposits. Willey Interscience, New York, pp 509–567
Ohmoto H (1986) Stable isotope geochemistry of ore deposits. In: Valley JW, Taylor HP, O'Neil JR (ed) Stable isotopes, Reviews in Mineralogy, vol 16, Mineralogical Society of America, pp 491–559
Ohmoto H (1996) Formation of volcanogenic massive sulphide deposits: the Kuroko perspective. Ore Geol Rev 10: 135–177
Papunen H (1966) Framboidal texture of the pyritic layer found in a peat bog in SE-Finland. CR Soc Geol Finland 38: 117–125
Pesquera A, Velasco F (1993) Ore metamorphism in sulfide mineralizations from the Cinco Villas massif (Western Pyrenees, Spain). Econ Geol 88: 266–282
Petersen S, Herzig PM, Hannington MD, Tichomirowa M (1997) The active TAG hydrothermal mound, Mid-Atlantic Ridge, 26°N: a Cyprus-type massive sulphide deposit at the modern seafloor. Proc Abstr SEG Field Conf 1997, Lisbon, Portugal, p 28
Quesada C (1991) Geological constraints on the Paleozoic tectonic evolution of tectostratigraphic terranes in the Iberian Massif. Tectonophysics 185: 225–245
Rambaud F (1969) El sinclinal carbonífero de Rio Tinto (Huelva) y sus mineralizaciones asociadas. Mem. IGME 71 (PhD Thesis, Universidad de Madrid), 230 p

Ramdohr P (1980) The ore minerals and their intergrowths. Pergamon Press, vol. I, 1205p
Ribeiro A, Silva JB (1983) Structure of South Portuguese Zone. Mem Serv Geol Port 29: 83–90
Robinson BW, Kusakabe M (1975) Quantitative preparation of SO2 for $^{34}S/^{32}S$ analysis from sulphides by combustion with cuprous oxide. Anal Chem 47: 1179–1181
Roedder E (1968) The noncolloidal origin of "colloform" textures in sphalerite ores. Econ Geol 63: 451–471
Routhier P, Aye F, Boyer C, Lècolle M, Molière P, Picot P, Roger G (1978) La Ceinture Sud–Ibérique à amas sulfurés dans sa partie espagnole mediane. Mém BRGM 94. 265 p
Rye OR, Ohmoto H (1974) Sulfur and carbon isotopes and ore genesis: a review. Econ Geol 69: 826–842
Sáez R, Almodóvar G (1993) An introduction to the ore geology of the Iberian Pyrite Belt. "In Fenoll P, Torres–Ruiz J, Gervilla F, Velasco–Roldán F (eds). Field–Trip Guide, Second Biennial SGA Meeting. University of Granada, Spain, pp 1–17
Sáez R, Almodóvar GR, Pascual E (1996) Geological constraints on massive sulphide genesis in the Iberian Pyrite Belt. Ore Geol Rev 11: 429–451
Sáez R, Pascual E, Toscano M, Almodóvar G (in press) The Iberian type of volcano-sedimentary massive sulphide deposits. In: Rickard D (ed) "Agrícola Volume – Mineral deposits of Europe", John Willey and Sons
Sánchez-España J, Velasco F, Yusta I (1997) Hydrothermal alteration geochemistry of some massive sulfide deposits at the Rio Tinto Syncline, Iberian Pyrite Belt, Spain. In: Papunen H (ed) 'Mineral deposits research and exploration. Where do they meet.?' Turku, Finland, pp 375–378
Sangster DF (1971) Sulphur isotopes, stratabound sulphide deposits, and ancient seas. Soc Mining Geol Japan, Spec Issue Proc IMA-IAGOD Meeting '70–3: 295–299
Sawkins FJ (1990) Metal deposits in relation to plate tectonics. 2nd edn . Springer Verlag, Berlin Heidelberg New York, 461 p
Schermerhorn LJG (1971) An outline stratigraphy of the Iberian Pyrite Belt. Bol Geol Miner 82: 239–268
Strauss GK (1970) Sobre la geología de la provincia piritífera del suroeste de la Península Ibérica y de sus yacimientos, en especial sobre la mina de pirita de Lousal (Portugal). Mem IGME 77, 266 p
Taylor GR (1982) A mechanism for framboid formation as illustrated by a volcanic exhalative sediment. Mineralium Deposita 17: 23–36
Thiéblemont D, Marcoux E, Tégyey M, Leistel JM (1994) Genèse de la province pyriteuse sud-ibérique dans un paléo-prisme d'accretion? Bull Soc Géol Fr 165: 407–423
Tornos F, González Clavijo E, Spiro B (1998) The Filón Norte massive sulphide orebody (Tharsis, Iberian Pyrite Belt): hydrothermal and tectonic evolution. Mineralium Deposita 33: 150–169
Toscano M, Ruiz de Almodóvar G, Pascual E, Sáez R (1993) Hydrothermal alteration related to the "Masa Valverde" massive sulphide deposit, Iberian Pyrite Belt, Spain. In: Fenoll Hach–Alí P, Torres–Ruiz J, Gervilla F (eds) Current research in geology applied to ore deposits. Granada, Spain, pp 389–392
Toscano M, Sáez R, Almodóvar GR (1997) Multi-stage fluid evolution in the Masa Valverde stockwork (Iberian Pyrite Belt): evidence from fluid inclusions. Proc Abstr SEG Field Conf, Lisbon, Portugal, pp 101
Wilkin RT, Barnes HL (1997) Formation processes of framboidal pyrite. Geoch em Cosmochim Acta 61–2: 323–339
Williams D, Stanton RL, Rambaud F (1975) The Planes–San Antonio pyritic deposit of Riotinto, Spain: its nature, environment and genesis. Trans Inst Min Metal1 84: B73–B82
Yamamoto M, Kase K, Carvalho D, Nakamura T, Mitsuno C (1993) Ore mineralogy and sulfur isotopes of the volcanogenic massive sulphide in the Iberian Pyrite Belt. Resour Geol Spec Iss 15: 67–80
Yui S, Ishitoya K (1983). Some textures of the ores from the Ezuri Kuroko deposits, Akita Prefecture, Japan. Econmic geology. In: Ohmoto H, Skinner BJ (eds) The Kuroko and related volcanogenic massive sulphide deposits. Econ Geol Monogr 5: 224–230
Zierenberg RA, Shanks WC (1988) Isotopic studies of epigenetic features in metalliferous sediment, Atlantis II Deep, Red Sea. Can Mineral 26–3: 737–754